GeoScienceWorld
Lithosphere
Volume 2022, Article ID 1939833, 12 pages
https://doi.org/10.2113/2022/1939833

Lithosphere

Research Article

Effect of Water Saturation on Gas-Accessible Effective Pore Space in Gas Shales

Lei Chen,[1,2,3] **Keyu Liu**,[1,2] **Liangwei Xu**,[4] **Shu Jiang**,[5] **Yonghong Fu**,[6] **Jingqiang Tan**,[7] **and Yuchen Fan**[2]

[1]*Shandong Provincial Key Laboratory of Deep Oil and Gas, China University of Petroleum (East China), Qingdao 266580, China*
[2]*School of Geosciences, China University of Petroleum (East China), Qingdao 266580, China*
[3]*Energy & Geoscience Institute, University of Utah, Salt Lake City, UT 84108, USA*
[4]*School of Earth and Space Sciences, Peking University, Beijing 100871, China*
[5]*Key Laboratory of Tectonics and Petroleum Resources, Ministry of Education, China University of Geosciences, Wuhan 430074, China*
[6]*School of Geoscience and Technology, Southwest Petroleum University, Chengdu 610500, China*
[7]*School of Geosciences and Info-Physics, Central South University, Changsha 410012, China*

Correspondence should be addressed to Lei Chen; chenlei19880804@163.com

Received 28 June 2022; Accepted 6 August 2022; Published 17 August 2022

Academic Editor: Qinghai Xu

The existence and content of water will certainly affect the effective pore space of shales and therefore is a key point for the evaluation of in-situ gas content and gas flow capacity of shale reservoirs. In order to reasonably evaluate the gas storage and flow capacities of water-bearing shale reservoirs, the effect of water on the effective pore space of shales needs to be understood. In this study, the Upper Permian Longtan shale in the southeastern Sichuan Basin, China, was selected as an example to conduct nuclear magnetic resonance cryoporometry (NMRC) measurements under different water saturation levels. The gas-accessible effective pore spaces in shales under different water saturation levels were quantified, and the effect of water saturation on gas-accessible effective pore space in shales was investigated. The results show that water plays an important role in the gas-accessible effective pore space of shales. When the Longtan shale increases from a dry state to a water saturation of 65%, 75%, and 90%, the gas-accessible effective pore volume decreases by 35%-60% (average 46.3%), 50%-70% (average 58.8%), and 65%-82% (average 75.8%), respectively. Water has an effect on the gas-accessible effective pore space regardless of pore size, and the effect is the strongest in the 4-100 nm range, which may be mainly due to the high content of clay minerals in the Longtan shale. Our studies are of important theoretical significance and application prospects for accurately evaluating the gas-accessible effective pore space of gas shales under actual geological conditions.

1. Introduction

In the early 21st century, the successful commercial development of Barnett shale gas in the United States made it widely recognized that the abundant natural gas resources were contained in shale pores, and then a "shale gas revolution" was set off in the energy field around the world [1–7]. In recent years, China has made significant breakthroughs in shale gas exploration and development, becoming the first country outside North America that achieved large-scale commercial development, and has achieved scale-efficient development in Fuling, Changning, Weiyuan, Zhaotong, and other areas [8, 9]. With the increasing proportion of natural gas in energy consumption and the successful commercial development of shale gas in the Southern Sichuan Basin, shale gas will become an important part of supporting the growth of natural gas production in China [10].

Compared with the conventional reservoirs, the shale reservoirs are usually dominated by nanopores, and shale gas is mainly stored in nanopores [11, 12]. At the same time, nanopores are the main channels for gas flow, which play an important role in the production of shale gas [13–15].

Therefore, the study of nanopore distribution characteristics is of great significance for the evaluation of shale gas resources and the prediction of shale gas productivity. The pore distribution characteristics, an important branch of shale gas reservoir research, have been widely studied by many scholars, and some basic issues and essential characteristics have been well understood [16–22]. However, the development characteristics of effective pores in shales are still unclear.

There are many factors affecting the development of effective pores in shales, and the water content of shales is one of the most important factors [14, 15, 23–28]. For example, Li et al. [25] studied the water distribution characteristic in shale clay and found that under a certain humidity condition (such as 0.98), the water distributes in different sized pores mainly as (1) capillary water in the small pores (<6 nm) and (2) water film in the larger pores. Feng et al. [24] studied water adsorption and its impact on the pore structure characteristics of shale clay and also found that under a certain moisture condition, the small pores (approximately <5 nm) are blocked with the capillary water and disappear on the apparent pore size distribution curves while large pores are only covered with the adsorbed water film. Sun et al. [26] studied the occurrence of irreducible water in gas shales and found that compared to the dry sample, the nonmicropore specific surface areas and micropore volumes of the moist sample are significantly reduced by an average value of 61% and 30%, respectively, and that the water averagely occupies 82% and 41% of the inorganic and organic nonmicropore specific surface areas, respectively, and 44% and 18% of the inorganic and organic micropore volumes, respectively. Zhu et al. [28] investigated the water-bearing characteristics and their influences on the reservoir capacity in terrestrial shale reservoirs and pointed out that water can damage the shale reservoir capacity significantly, which is realized by decreasing its pore volume and specific surface area, up to 1/2 and 1/3, respectively. Specific surface area is more susceptible to water than pore volume due to its smaller variation range of pore size distribution (2.5-20 nm). Cheng et al. [23] studied the differences in the distribution and occurrence phases of pore water in various nanopores of marine-terrestrial transitional shales in the Yangquan area of the northeast Qinshui Basin and pointed out that the pore water takes up the majority of the inorganic-matter hosted pore structures, especially for the inorganic-matter hosted nonmicropore surfaces; however, it only occupies a few of the organic-matter hosted micropore structures and fails to occupy the organic-matter hosted nonmicropore structures. Xu et al. [27] studied the storing characteristics of connate water in lower Paleozoic shales in southeast Chongqing and pointed out that connate water occurs in shale micropores and nonmicropores, and adsorption and filing states simultaneously exist and are distributed in <10 nm mesopores and 0.4-0.6 nm micropores; this distribution reduces the pore structure parameters of inorganic matter in shale, especially the nonmicropore surface area.

The current geological analysis results reveal that under original formation conditions, actual shale reservoirs generally have a certain water saturation [29, 30]. The average water saturation of shale gas reservoirs in Barnett, Marcellus, and Woodford formations in the US ranges from 15% to 35% [31], compared to 30%-95% for the marine shale plays found in South China [32]. Under geological conditions, pore water in shales exists in various forms, for instance, it can be condensed in micropores, adsorbed on the surface of mesopores and macropores, or filled in pore spaces in a vapor state [33, 34]. Moreover, it can exist in both organic and inorganic pores [6, 35–37]. Pore water not only occupies the pore volume of shales but also blocks some pores, which significantly affects the gas-accessible effective pore space of shales [25, 38], thereby reducing the shale gas storage and flow capacities. For example, Merkel et al. [39] studied the methane adsorption capacity of shales in North America and argued that, compared to dry condition, a reduction of 54% and 72% in methane adsorption capacity was observed, respectively, in Haynesville Shale whose water saturation is 32% and Bossier Shale whose water saturation is 50%. Li et al. [40] pointed out that increased water saturation reduces the gas flow capacity, and when the water saturation is 40%, the gas flow capacity will decrease by about 20% compared to dry condition.

In summary, pore water has an important influence on the effective pore space of shales, thereby affecting the gas storage and flow capacities. However, dry samples are typically used in the current researches on the pore distribution characteristics of shales, without taking into account the influence of water content in shales [19, 41–43]. Therefore, the study on the distribution characteristics of effective pore spaces in shales under different water saturation levels is of important significance for more accurate evaluation of in situ gas content and gas flow capacity in shale reservoirs. This necessitates the study of how water saturation affects the gas-accessible effective pore space in gas shales.

Although some scholars have analyzed the influence of water on the pore space in shales, some details of the gas-accessible effective pore spaces at different water saturation levels are not well understood. In particular, the effect of water saturation on gas-accessible effective pore space in gas shales has not been illustrated. In this study, in order to solve the above problems, the Upper Permian Longtan shale in the southeastern Sichuan Basin, China, was selected as an example to conduct nuclear magnetic resonance cryoporometry (NMRC) measurements under different water saturation levels. The gas-accessible effective pore spaces in shales under different water saturation levels were quantified, and the effect of water saturation on gas-accessible effective pore space in shales was investigated. Our studies are of important theoretical significance and application prospects for accurately evaluating the gas-accessible effective pore space in gas shales and are of important guiding significance for the reasonable evaluation of shale gas storage and flow capacities under actual geological conditions.

2. Theoretical Basis

The NMRC method is a pore measurement method that uses nuclear magnetic resonance (NMR) technology to capture the phase transition process of probe liquid in pores and

uses Gibbs-Thomson equation to characterize the pore size distribution of porous material [44–47]. Gibbs-Thomson thermodynamic equation is the theoretical basis of the NMRC method, which establishes the relationship between the phase transition process of probe liquid in pores and pore size. After selecting the appropriate probe liquid, the pore size distribution of the material can be obtained by recording the phase transition of probe liquid in the porous material [48, 49]. At present, NMRC has been used in the pore characterization of various micro- and mesoporous materials [49–55]. Gibbs-Thomson equation for the melting point depression (ΔT_m) for a small crystal of diameter x is given by

$$\Delta T_m = T_m - T_m(x) = \frac{4\sigma_{sl} T_m}{x \Delta H_f \rho_s}, \quad (1)$$

where T_m is the bulk melting point of the solid, $T_m(x)$ is the melting point for crystals of diameter x, σ_{sl} is the surface energy at the liquid-solid interface, ΔH_f is the bulk enthalpy of fusion (per gram of material), and ρ_s is the density of the solid.

In formula (1), all items except diameter x are physical property parameters. For the same substance, they can be regarded as constant within the experimental temperature range; so, the above formula can be simplified as

$$\Delta T_m = \frac{K_{\mathrm{GT}}}{x}, \quad (2)$$

where K_{GT} is the melting point depression constant, which is related to the properties of probe liquid.

According to formula (2), the smaller the pore size, the lower the melting point and the more significant the change in melting point. The increase in the NMR signal intensity of probe liquid with temperature can be regarded as the accumulation of pore volume from small pores to large pores. Therefore, the pore size distribution of porous material can be obtained by measuring the liquid signal intensity in material during the temperature transition process. The phase transition process of probe liquid in the pores of porous material is shown in Figure 1. In this study, water was selected as the probe liquid, and the NMR signal intensity of water was measured and recorded in the sample melting process using the step nonisothermal method. Fitting of experiment data yields the plot of liquid signal intensity (I) with temperature (T), i.e., the I-T curve.

Based on this I-T curve, the pore size distribution can be obtained as follows: firstly, the NMR signal intensity I is converted to the volume of water (V); secondly, the temperature T is converted to diameter x using formula (2); finally, the relative change of water volume V (cumulative pore volume smaller than diameter x) to pore diameter x, $V(x)$, is obtained. Then, the formula for calculating the pore size distribution of the sample is expressed as

$$\frac{dV(x)}{d\lg(x)} = \frac{dV(x)}{d(x)} \cdot \frac{d(x)}{d\lg(x)} = \frac{dV(x)}{dx} \cdot x \cdot \ln 10. \quad (3)$$

3. Samples and Methods

3.1. Geological Setting and Samples. The organic-rich shale of Upper Permian Longtan Formation in the southeastern Sichuan Basin, China, is developed with large thickness, few interlayers, and moderate burial depth [56]. The quality of shale has the four high characteristics of "high clay minerals content, high porosity, high TOC content, and high gas content." The thermal maturity reaches a mature stage which is mainly in the dry gas window stage and indicates that the Longtan shale has good potential for shale gas [3]. Therefore, the Longtan shale in this area is one of the most favorable sweet spots for the exploration of marine-continental transitional shale gas in the Sichuan Basin in the near future.

In this study, four marine-continental transitional shale samples were collected from the Upper Permian Longtan Formation in the southeastern Sichuan Basin, China. The thermal maturity values for four shale samples range from 1.92% to 2.41% with an average of 2.24%, which suggests that the studied shale samples have entered the stage of dry gas window. Sample information such as ID and depth are listed in Table 1.

3.2. NMRC Measurements. In this study, for NMRC measurements, an NMRC 12-010 V instrument manufactured by Niumag Corporation Ltd., China, was used. The diagram of the instrument is shown in Figure 2, and the detailed parameters of the instrument can be found in Liu et al. [50] and Fu et al. [57].

The NMRC process for measuring the pore size distribution of shales in this study was divided into the next three steps. The first step is sample preparation and treatment. Firstly, the shale samples were crushed to 35-60 mesh, and then the crushed sample was weighed 2-3 g into a NMRC test tube, dried for 24 h, then weighed (M1), then placed in a vacuum tank for 12 h, and then saturated by deionized water at 25 MPa. After 24 h, the sample was taken out and weighed (M2) after removing floating water on the surface of the sample with a dry sponge. This means that the weight of water in the shale sample under saturated water condition is M2-M1.

The second step is the NMRC measurement under saturation water condition. It is necessary to establish the relationship between water volume and NMR signal intensity in order to obtain the pore size distribution of shales. As shown in Figure 3, the NMR signal intensity linearly correlates with water volume. Firstly, the NMR signal intensities were measured at temperatures less than 0°C and greater than 0°C, respectively, and then the relationship between temperature and NMR signal intensity was calibrated. The test temperature ranges from -26°C to -0.1°C, between which 28 temperature points with different steps were set, i.e., 1°C step from -26°C to -3°C, 0.5°C step from -3°C to -1°C, and 0.1°C step from -1°C to -0.1°C. Under saturation water condition, the NMRC measurement was carried out accordingly as follows: each test temperature was set stable for more than 30 min, followed by 3 to 5 minutes of test time. In such a way, the pore size distribution could be obtained by measuring the NMR signal intensity at different temperatures till all the ice in pores melt.

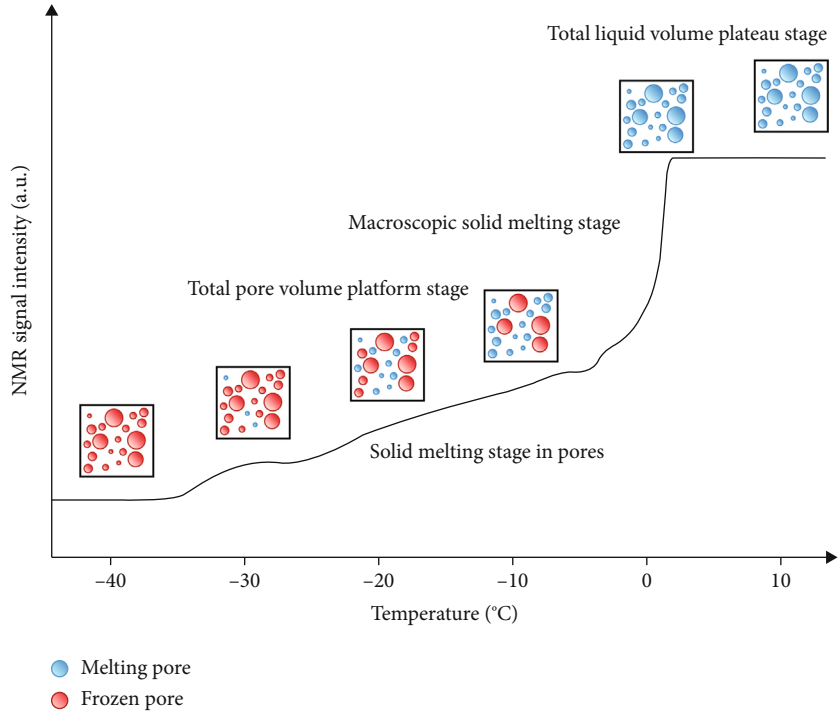

Figure 1: Phase transition process of probe liquid in the porous material (modified from [44]).

Table 1: Depth, TOC content, and mineralogical composition of four shale samples.

Sample ID	Depth (m)	TOC (%)	Mineralogical composition relative percent (%)				
			Quartz+feldspar	Carbonates	Pyrite	Total clays	Others
L-1	3096.0	3.27	15.6	18.1	5.1	56.0	5.2
L-2	3124.6	4.09	19.4	27.9	7.3	38.8	6.6
L-3	3134.4	6.36	26.0	4.9	6.0	58.2	4.9
L-4	3154.9	3.95	27.0	3.8	7.3	56.2	5.7

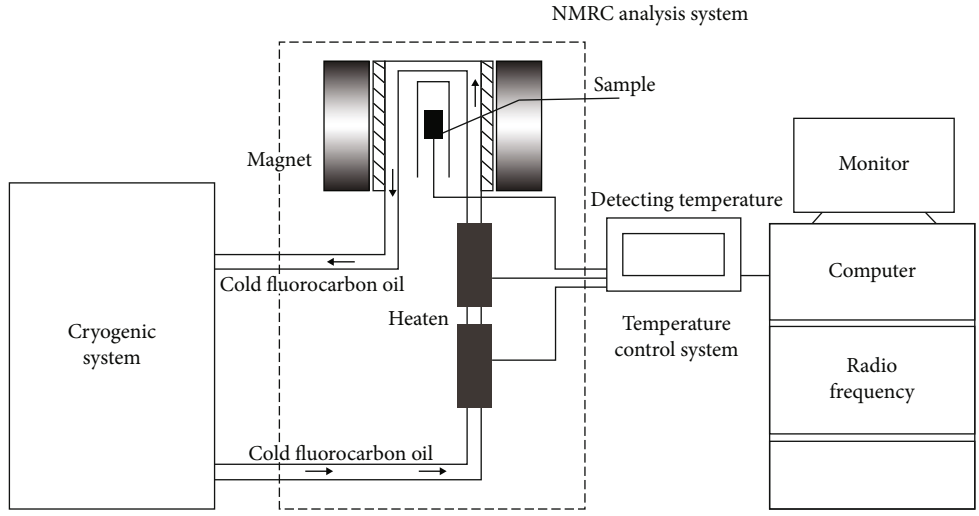

Figure 2: Diagram of the NMRC analyzer.

The third step is the NMRC measurement under different water saturation levels. Upon completion of step 2, the sample was taken out and dried at 60°C whilst weighed every 10 seconds until reaching 0.9 M2 + 0.1 M1 (note that the error could be no more than 0.0002 g), at which point water saturation was 90% exact. It should be noted here that since

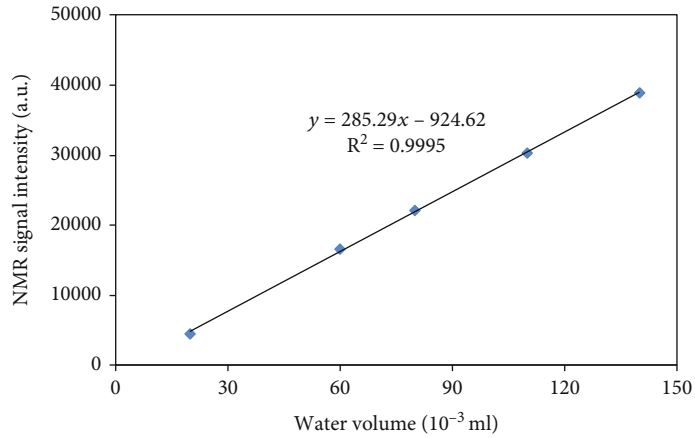

Figure 3: Linear correlation between water volume and NMR signal intensity.

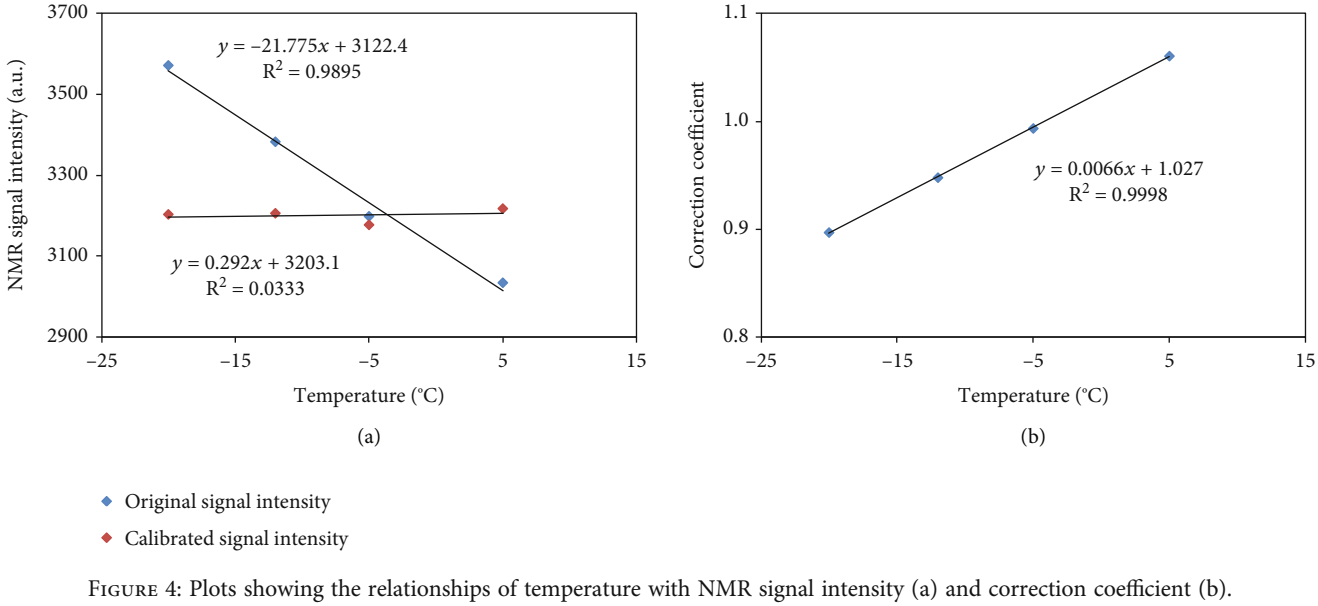

Figure 4: Plots showing the relationships of temperature with NMR signal intensity (a) and correction coefficient (b).

the weight of water in the water-bearing shale sample is reduced by 10%, the weight of the water-bearing shale sample at this time is M1+0.9 (M2-M1), which is 0.9 M2 + 0.1 M1. At the same time, the water saturation of the sample is 90%. According to the above principle and method, the measurement was carried out for water saturation of 75% and 65%, respectively.

It should be noted that in the NMRC measurement, the temperature variation will affect the physical properties of samples and NMRC probe, which could also influence the NMR signal intensity and the accuracy of temperature control, bringing errors to the experimental results [52]. In particular, a small temperature variation close to 0°C might cause a significant shift of pore size distribution. Therefore, it is necessary to calibrate the original signal intensity. Firstly, specific temperature points including less than 0°C and greater than 0°C were selected, and their NMR signal intensities were calibrated to that measured at 0°C (Figure 4(a)). Then, the correction coefficient was obtained by the ratio of the original signal intensity to the calibrated signal intensity; thereafter, the relationship between the correction coefficient and temperature was established (Figure 4(b)). Finally, the correction coefficients at other temperatures were obtained through the corresponding relationship, and then the calibrated NMR signal intensities were obtained.

4. Results and Discussion

4.1. Characteristics of NMRC Results. The water-accessible cumulative pore volumes of four shale samples under different water saturation levels are shown in Figure 5. It can be clearly seen that the water-accessible cumulative pore volume shows a significant decreasing trend with decreasing water saturation, which is mainly due to the fact that as water gradually escapes from the pores, the remaining water-accessible pore volume will inevitably gradually decrease. When water saturation changes from one to another, the reduction of pore volume occupied by water is inconsistent for different samples, which is mainly associated with different TOC contents and mineralogical compositions of the shale samples.

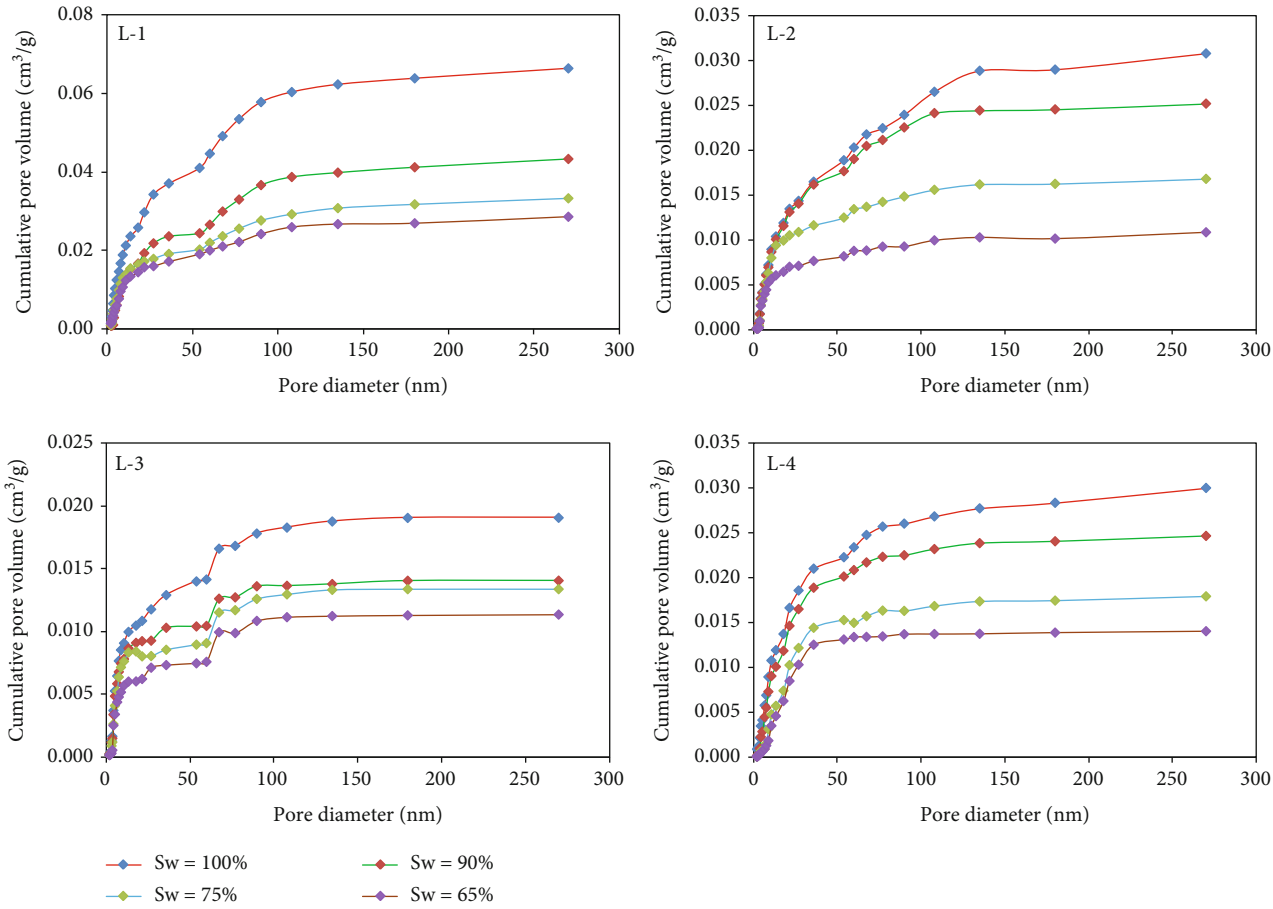

Figure 5: Water-accessible cumulative pore volumes of four shale samples under different water saturation levels.

The water-accessible pore size distributions of four samples under different water saturation levels calculated from Figure 5 are shown in Figure 6. Overall, the water-accessible pore size distribution curve with low water saturation falls below that with high water saturation. In addition, the water-accessible pore size distributions are complicated, and all curves have multimodal characteristics.

4.2. Effect of Water Saturation on Gas-Accessible Effective Pore Space. The nanopores in shales are the main storage space of shale gas [41]. The pore volume directly determines the free gas storage capacity of shales, and free gas content is directly related to the productivity and production rate of shale gas wells [9]. Under water-bearing condition, water is adsorbed on the pore surface and occupies a certain pore volume, reducing the pore surface for gas adsorption and pore volume for gas storage [58]. The gas-accessible cumulative pore volumes of four shale samples under different water saturation levels calculated from Figure 5 are shown in Figure 7. It should be noted that since the water-accessible pore space measured under saturated water condition is the total pore space of the shale sample, it can be regarded as the gas-accessible pore space of the shale sample under dry condition. Therefore, the water saturation values of 100% in Figures 5 and 6 were changed to the water saturation values of 0 in Figures 7 and 8.

As observed from Figure 7, the gas-accessible effective pore volume shows a significant decreasing trend with increasing water saturation. For example, the pore volume of sample L-1 under dry condition is 0.0664 cm^3/g, and when the water saturation increases to 65%, 75%, and 90%, the gas-accessible effective pore volume decreases to 0.0378 cm^3/g, 0.0331 cm^3/g, and 0.0231 cm^3/g, with a decrease range of 43%, 50%, and 65%, respectively. Similarly, the gas-accessible effective pore volume of sample L-2 is reduced by 35%, 55%, and 82%, that of L-3 reduced by 60%, 70%, and 74%, and that of L-4 reduced by 47%, 60%, and 82%, respectively. In summary, when the Longtan shale increases from a dry state to a water saturation of 65%, 75%, and 90%, the gas-accessible effective pore volume decreases by 35%-60% (average 46.3%), 50%-70% (average 58.8%), and 65%-82% (average 75.8%), respectively. The presence of water has a significant influence on the gas-accessible effective pore volume of shales. When the sample changes from dry condition to the same water saturation, the reduction of gas-accessible effective pore volume is inconsistent for different samples, which is mainly associated with different TOC contents and mineralogical compositions of the shale samples.

The gas-accessible pore size distributions of four shale samples at different water saturation levels calculated from Figure 6 are shown in Figure 8. Overall, the gas-accessible

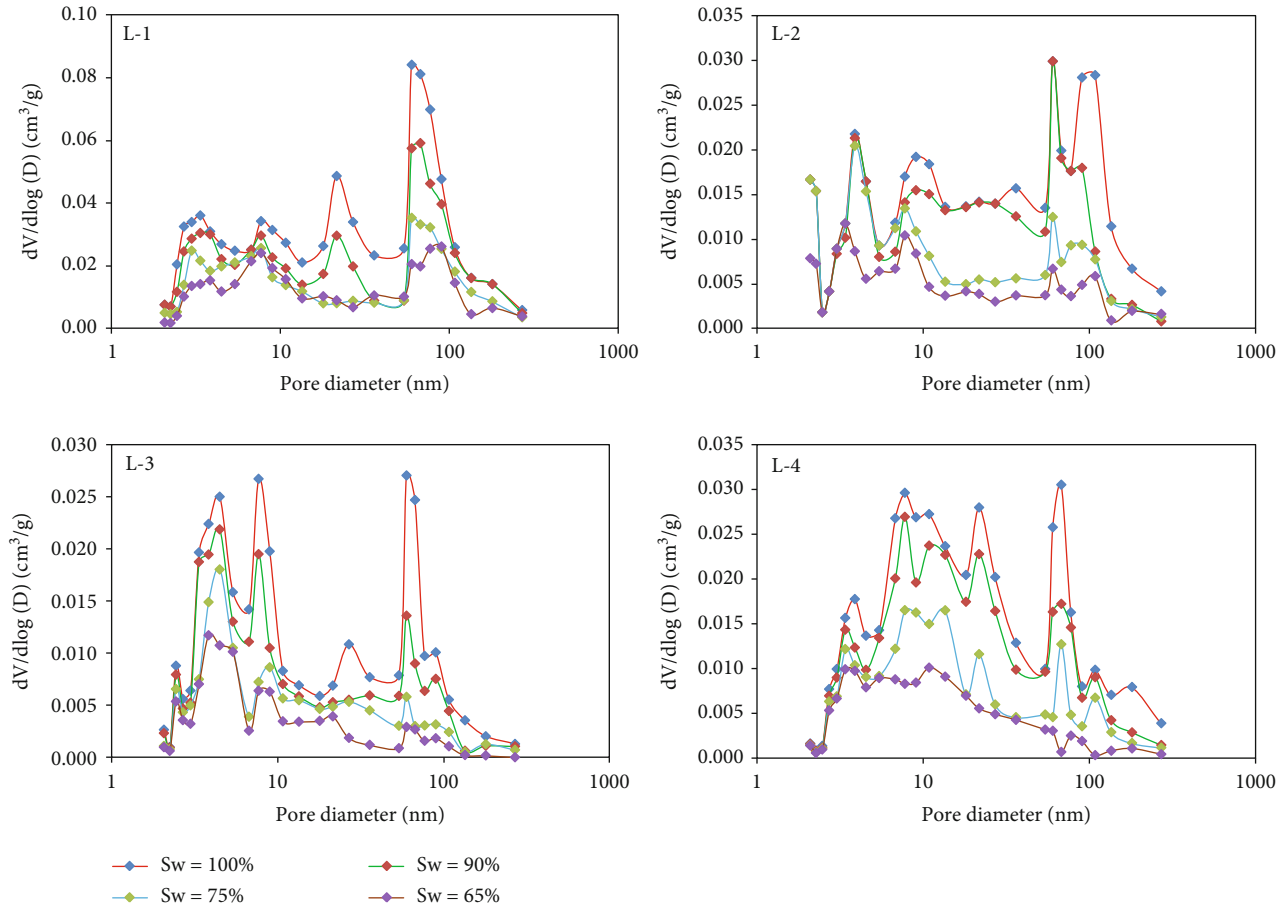

Figure 6: Water-accessible pore size distributions of four shale samples under different water saturation levels.

pore size distribution curve with low water saturation falls above that with high water saturation. In addition, the gas-accessible pore size distributions are complicated, and all curves have multimodal characteristics. Water has an effect on the gas-accessible effective pore space regardless of pore size, and the effect is the strongest in the 4-100 nm range, which may be mainly due to the high content of clay minerals in the Longtan shale. Clay minerals develop multiscale pore networks and have strong hydrophilicity [28, 59]; so, when water enters their pores, pores of all sizes will be filled very quickly. Therefore, it can be found that the presence of water significantly affects the gas-accessible effective pore space of shales, thereby reducing the contribution of pore space to shale gas storage and flow capacities.

4.3. Advantages and Limitations of the NMRC Approach. Compared with mercury intrusion porosimetry (MIP), low-pressure nitrogen adsorption (LPNA), and NMR methods, the NMRC measurement has its unique advantages [54, 60]. In the MIP method, excessive intrusion pressure may cause damage to the pore structure of the sample [52], while the probe liquid in the NMRC method mainly relies on spontaneous imbibition during the process of saturating the pores of the sample and will not destroy the pore structure [61]. In addition, the MIP method measures the pore throat size rather than the pore size [50], while the NMRC method directly measures the pore size [46, 47]. Compared with the LPNA method, the advantage of the NMRC method is that it can measure the pores in shale reservoirs with a larger diameter range (2-300 nm), and the test results are not controlled by the constraints of different algorithms. In addition, the advantage of the NMRC method is that its theoretical basis is the Gibbs-Thomson equation, which can directly reveal the relationship between melting point and pore volume. Therefore, the complex pore structure of shale reservoirs has little effect on this method [46, 47], but it has a greater influence on the LPNA method which depends on different algorithms [52]. Compared with the NMR method, the NMRC method measures the smaller pore size of shale reservoirs and reveals more detailed information about the pore size distribution characteristics [45]. Moreover, the NMRC method also has other advantages that many methods such as MIP and LPNA do not have, such as no contamination of the sample, no damage to the pore structure of the sample, and convenient and fast testing.

In addition to the above advantages, more importantly, the NMRC method can accurately characterize the effective pore spaces of shales under different water saturation levels. At present, the MIP and LPNA methods are mainly used to characterize the pore space of shales under dry condition [16, 22, 42]. When shale contains a certain amount of water, for the MIP method, mercury may displace the water in

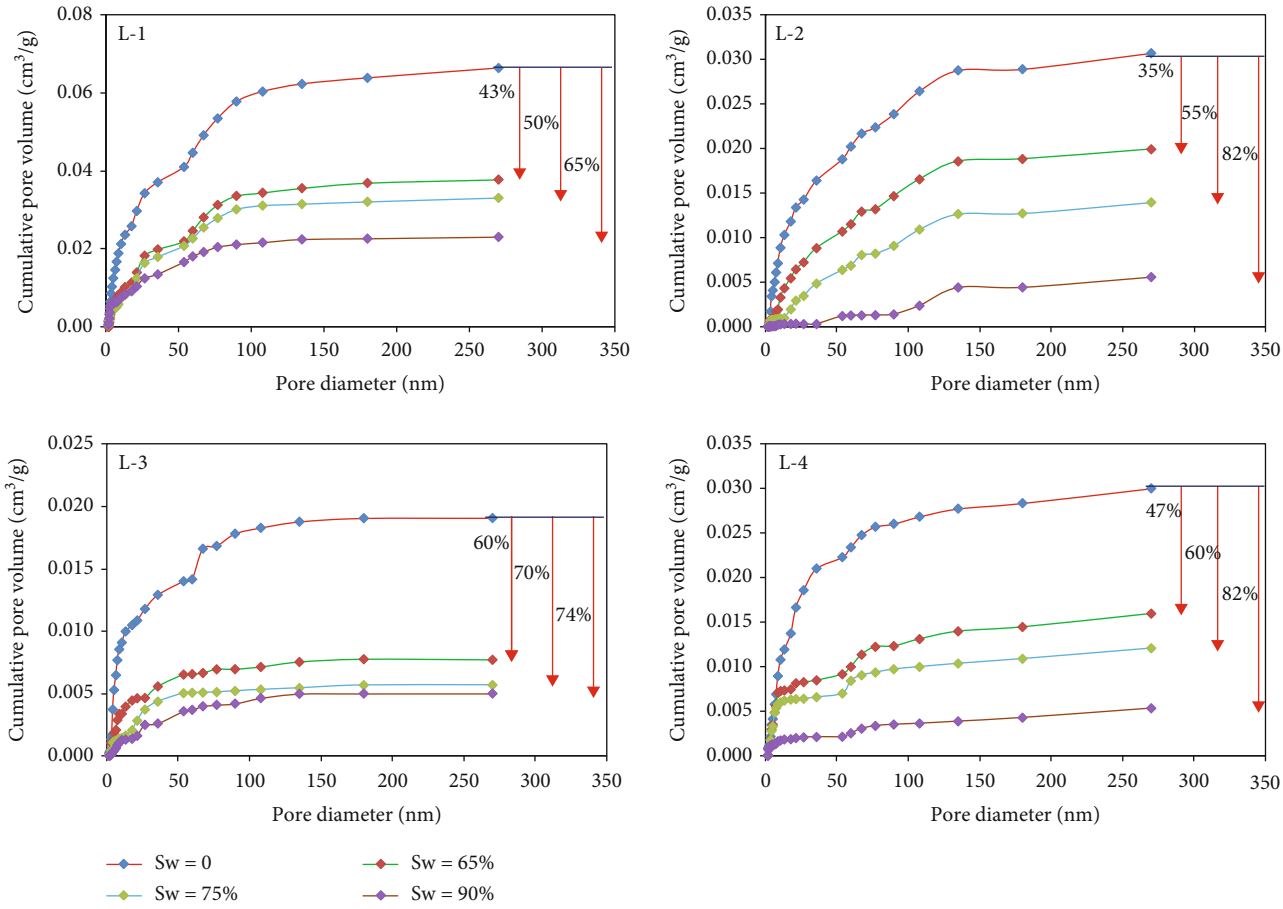

Figure 7: Gas-accessible cumulative pore volumes of four shale samples under different water saturation levels.

pores under high pressure, which makes it impossible to accurately characterize the effective pore space of shales under water-bearing condition; for the LPNA method, due to experiments, vacuuming is required beforehand, which will inevitably remove the water in pores of shales, and it is also impossible to accurately characterize the effective pore space of shales under water-bearing condition. In summary, the NMRC method has unique advantages in characterizing the effective pore size distribution of shales under water-bearing condition. It can not only quantify the gas-accessible effective pore space of shales under water-bearing condition but also clarify the effect of water saturation on gas-accessible effective pore space in gas shales. Therefore, this approach is more effective and efficient for the quantification of the gas-accessible effective pore space in gas shales compared to other approaches.

Nevertheless, this method has its own limitations [62]. Firstly, shale reservoirs usually have smaller porosity and pore size than conventional reservoirs and may contain paramagnetic materials, resulting in low signal-to-noise ratio and short relaxation time of NMRC experimental results, which will affect the test accuracy to a certain extent. Secondly, the selection of NMRC experimental parameters will directly affect the reliability of the analysis results, and further research is needed to determine reasonable experimental parameters. Finally, nanopores have significant scale effects on the thermodynamic properties of fluids, especially for materials with pore diameters less than 10 nm. Therefore, theoretical models such as Gibbs-Thomson equation need to be improved and supplemented. In addition, the NMRC method cannot effectively characterize the micropores of porous materials, and the effective micropore spaces of shales under different water saturation levels will be investigated in the near future.

4.4. Significance for the In Situ Shale Gas Content Evaluation. The nanopores developed in shale reservoirs are the main space for gas occurrence and the main channel for gas flow [17]. The current evaluation of pore space in shales is mainly based on dry condition; however, the actual shale reservoirs generally have a certain water, which occupies a certain pore space. Therefore, how to quantitatively characterize the effective pore space of shales under water-bearing condition is of great significance for the scientific and reasonable evaluation of in situ shale gas content and shale gas resource potential.

In this study, the NMRC measurements were conducted under different water saturation levels. The gas-accessible effective pore spaces in shales under different water saturation levels were quantified, and the effect of water saturation on gas-accessible effective pore space in shales was investigated. These studies are beneficial to further understand the effective pore space of shales under original formation

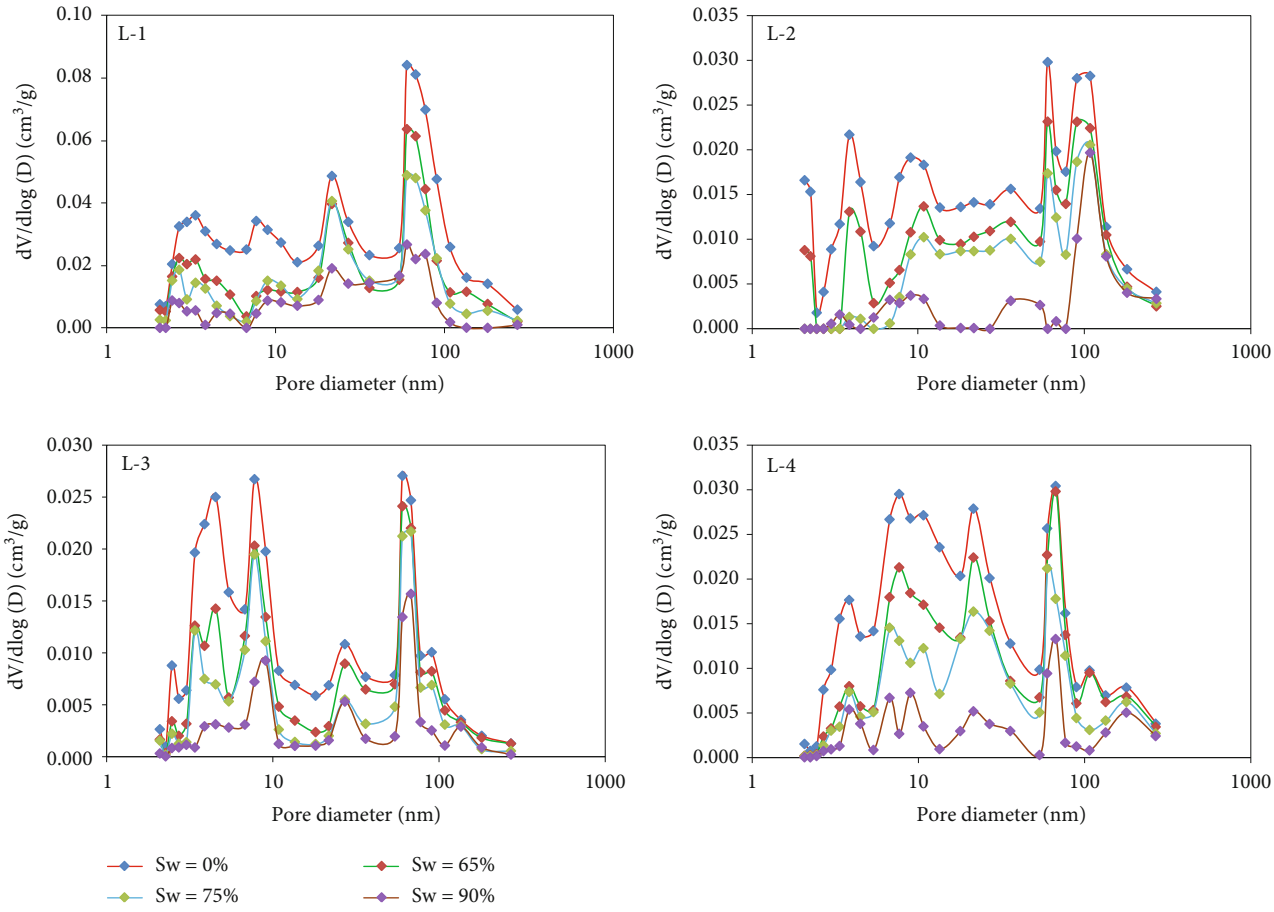

Figure 8: Gas-accessible pore size distributions of four shale samples under different water saturation levels.

conditions, thereby further improving the accuracy of shale gas content evaluation under actual geological conditions, and guiding shale gas exploration and development.

In the process of shale gas exploitation, the existence of water will inevitably affect the gas flow law in nanopores of shales [40]. Therefore, quantitative analysis of the influence of water on the effective pore space in shales is of great guiding significance for shale gas productivity prediction.

5. Conclusions and Suggestion

This study showcases a novel approach to quantify the gas-accessible effective pore spaces of shales under different water saturation levels using the NMRC measurements. This analytical approach has been successfully applied to four Upper Permian Longtan shale samples with multiscale pore structures. The following are the main conclusions in this study:

(1) When the Longtan shale increases from a dry state to a water saturation of 65%, 75%, and 90%, the gas-accessible effective pore volume decreases by 35%-60% (average 46.3%), 50%-70% (average 58.8%), and 65%-82% (average 75.8%), respectively

(2) Water has an effect on the gas-accessible effective pore space regardless of pore size, and the effect is the strongest in the 4-100 nm range, which may be mainly due to the high content of clay minerals in the Longtan shale

In future work, the effective micropore spaces of shales under different water saturation levels will be investigated to deepen the understanding of the effective pore space in shales and further guide the in situ shale gas content evaluation.

Data Availability

The data that support the findings of this study are available from the corresponding author (Lei Chen) upon reasonable request.

Conflicts of Interest

The authors declare no conflicts of interest.

Acknowledgments

The authors would like to acknowledge the financial support of the Natural Science Foundation of Shandong Province (No. ZR2021QD057), the National Postdoctoral Program for Innovative Talent (No. BX20190387), China

Postdoctoral Science Foundation (No. 2020M682262), and the Fundamental Research Funds for Central Universities (No. 20CX06014A). Special thanks are given to the China Scholarship Council (No. 201706440133) for sponsoring the first author to be a visiting scholar in the University of Utah.

References

[1] L. Chen, K. Y. Liu, S. Jiang, H. X. Huang, J. Q. Tan, and L. Zuo, "Effect of adsorbed phase density on the correction of methane excess adsorption to absolute adsorption in shale," *Chemical Engineering Journal*, vol. 420, article 127678, 2021.

[2] C. Frohlich and M. Brunt, "Reprint of: two-year survey of earthquakes and injection/production wells in the Eagle Ford Shale, Texas, prior to theMW4.820 October 2011 earthquake," *Earth and Planetary Science Letters*, vol. 402, pp. 257–264, 2014.

[3] X. S. Guo, D. F. Hu, R. B. Liu, X. F. Wei, and F. B. Wei, "Geological conditions and exploration potential of Permian marine-continent transitional facies shale gas in the Sichuan Basin," *Natural Gas Industry B*, vol. 6, no. 3, pp. 198–204, 2019.

[4] H. X. Huang, R. X. Li, Z. Lyu et al., "Comparative study of methane adsorption of Middle-Upper Ordovician marine shales in the western Ordos Basin, NW China: insights into impacts of moisture on thermodynamics and kinetics of adsorption," *Chemical Engineering Journal*, vol. 446, article 137411, 2022.

[5] D. M. Jarvie, R. J. Hill, T. E. Ruble, and R. M. Pollastro, "Unconventional shale-gas systems: the Mississippian Barnett shale of north-Central Texas as one model for thermogenic shale-gas assessment," *AAPG Bulletin*, vol. 91, no. 4, pp. 475–499, 2007.

[6] D. J. K. Ross and R. M. Bustin, "The importance of shale composition and pore structure upon gas storage potential of shale gas reservoirs," *Marine and Petroleum Geology*, vol. 26, no. 6, pp. 916–927, 2009.

[7] C. N. Zou, Z. Yang, S. S. Sun et al., ""Exploring petroleum inside source kitchen": shale oil and gas in Sichuan Basin," *Science China Earth Sciences*, vol. 63, no. 7, pp. 934–953, 2020.

[8] S. K. Gao, D. Z. Dong, K. Tao, W. Guo, X. J. Li, and S. R. Zhang, "Experiences and lessons learned from China's shale gas development: 2005-2019," *Journal of Natural Gas Science and Engineering*, vol. 85, article 103648, 2021.

[9] X. H. Ma, J. Xie, R. Yong, and Y. Q. Zhu, "Geological characteristics and high production control factors of shale gas reservoirs in Silurian Longmaxi formation, southern Sichuan Basin, SW China," *Petroleum Exploration and Development*, vol. 47, no. 5, pp. 901–915, 2020.

[10] S. Z. Li, Z. Zhou, H. K. Nie et al., "Distribution characteristics, exploration and development, geological theories research progress and exploration directions of shale gas in China," *China Geology*, vol. 5, pp. 110–135, 2022.

[11] L. Chen, Z. X. Jiang, Q. X. Liu et al., "Mechanism of shale gas occurrence: insights from comparative study on pore structures of marine and lacustrine shales," *Marine and Petroleum Geology*, vol. 104, pp. 200–216, 2019.

[12] L. Chen, L. Zuo, Z. X. Jiang et al., "Mechanisms of shale gas adsorption: evidence from thermodynamics and kinetics study of methane adsorption on shale," *Chemical Engineering Journal*, vol. 361, pp. 559–570, 2019.

[13] K. L. Wu, Z. X. Chen, X. F. Li et al., "Flow behavior of gas confined in nanoporous shale at high pressure: real gas effect," *Fuel*, vol. 205, pp. 173–183, 2017.

[14] L. H. Zhang, H. B. Liang, Y. L. Zhao, J. Xie, X. Peng, and Q. Li, "Gas transport characteristics in shale matrix based on multiple mechanisms," *Chemical Engineering Journal*, vol. 386, article 124002, 2020.

[15] Y. X. Zhang, Q. H. Hu, T. J. Barber, M. Bleuel, L. M. Anovitz, and K. Littrell, "Quantifying fluid-wettable effective pore space in the Utica and Bakken oil shale formations," *Geophysical Research Letters*, vol. 47, no. 14, article e2020GL087896, 2020.

[16] L. Chen, Z. X. Jiang, K. Y. Liu, J. Q. Tan, F. L. Gao, and P. F. Wang, "Pore structure characterization for organic-rich lower Silurian shale in the Upper Yangtze Platform, South China: a possible mechanism for pore development," *Journal of Natural Gas Science and Engineering*, vol. 46, pp. 1–15, 2017.

[17] R. Fink, A. Amann-Hildenbrand, P. Bertier, and R. Littke, "Pore structure, gas storage and matrix transport characteristics of lacustrine Newark shale," *Marine and Petroleum Geology*, vol. 97, pp. 525–539, 2018.

[18] Z. Y. Gao, Y. P. Fan, Q. X. Xuan, and G. W. Zheng, "A review of shale pore structure evolution characteristics with increasing thermal maturities," *Advances in Geo-Energy Research*, vol. 4, no. 3, pp. 247–259, 2020.

[19] M. Garum, P. W. J. Glover, P. Lorinczi, R. Drummond-Brydson, and A. Hassanpour, "Micro- and nano-scale pore structure in gas shale using Xμ-CT and FIB-SEM techniques," *Energy & Fuels*, vol. 34, no. 10, pp. 12340–12353, 2020.

[20] K. J. Li, S. Q. Kong, P. Xia, and X. L. Wang, "Microstructural characterisation of organic matter pores in coal-measure shale," *Advances in Geo-Energy Research*, vol. 4, no. 4, pp. 372–391, 2020.

[21] M. Pommer and K. Milliken, "Pore types and pore-size distributions across thermal maturity, Eagle Ford Formation, southern Texas," *AAPG Bulletin*, vol. 99, no. 9, pp. 1713–1744, 2015.

[22] L. W. Xu, K. J. Yang, L. F. Zhang, L. F. Liu, Z. X. Jiang, and X. Li, "Organic-induced nanoscale pore structure and adsorption capacity variability during artificial thermal maturation: pyrolysis study of the Mesoproterozoic Xiamaling marine shale from Zhangjiakou, Hebei, China," *Journal of Petroleum Science and Engineering*, vol. 202, article 108502, 2021.

[23] P. Cheng, X. M. Xiao, H. Tian et al., "Differences in the distribution and occurrence phases of pore water in various nanopores of marine-terrestrial transitional shales in the Yangquan area of the northeast Qinshui Basin, China," *Marine and Petroleum Geology*, vol. 137, article 105510, 2022.

[24] D. Feng, X. F. Li, X. Z. Wang et al., "Water adsorption and its impact on the pore structure characteristics of shale clay," *Applied Clay Science*, vol. 155, pp. 126–138, 2018.

[25] J. Li, X. F. Li, X. Z. Wang et al., "Water distribution characteristic and effect on methane adsorption capacity in shale clay," *International Journal of Coal Geology*, vol. 159, pp. 135–154, 2016.

[26] J. Sun, X. M. Xiao, Q. Wei, P. Cheng, and H. Tian, "Occurrence of irreducible water and its influences on gas-bearing property of gas shales from shallow Longmaxi formation in the Xishui area, Guizhou, southern China," *Frontiers in Earth Science*, vol. 9, article 654136, 2021.

[27] L. W. Xu, H. Wei, L. Chen et al., "Storing characteristics and main controlling factors of connate water in lower Paleozoic

shales in southeast Chongqing, China," *Journal of Petroleum Science and Engineering*, vol. 215, article 110543, 2022.

[28] H. J. Zhu, C. Huang, Y. W. Ju et al., "Multi-scale multi-dimensional characterization of clay-hosted pore networks of shale using FIBSEM, TEM, and X-ray micro-tomography: implications for methane storage and migration," *Applied Clay Science*, vol. 213, article 106239, 2021.

[29] P. Cheng, X. M. Xiao, X. Wang, J. Sun, and Q. Wei, "Evolution of water content in organic-rich shales with increasing maturity and its controlling factors: Implications from a pyrolysis experiment on a water- saturated shale core sample," *Marine and Petroleum Geology*, vol. 109, pp. 291–303, 2019.

[30] Y. Mu, Z. M. Hu, R. Shen et al., "Water occurrence characteristics of gas shale based on 2D NMR technology," *Energy & Fuels*, vol. 36, no. 2, pp. 910–921, 2022.

[31] R. J. Ambrose, R. C. Hartman, M. Diaz-Campos, I. Y. Akkutlu, and C. H. Sondergeld, "Shale gas-in-place calculations part I: new pore-scale considerations," *SPE Journal*, vol. 17, no. 1, pp. 219–229, 2012.

[32] H. L. Liu and H. Y. Wang, "Ultra-low water saturation characteristics and the identification of over-pressured play fairways of marine shales in South China," *Natural Gas Industry*, vol. 33, pp. 140–144, 2013.

[33] D. B. Bennion and F. B. Thomas, "Formation damage issues impacting the productivity of low permeability, low initial water saturation gas producing formations," *Journal of Energy Resources Technology*, vol. 127, no. 3, pp. 240–247, 2005.

[34] P. Cheng, H. Tian, X. M. Xiao, H. F. Gai, T. F. Li, and X. Wang, "Water distribution in overmature organic-rich shales: implications from water adsorption experiments," *Energy & Fuels*, vol. 31, no. 12, pp. 13120–13132, 2017.

[35] G. R. Chalmers, R. M. Bustin, and I. M. Power, "Characterization of gas shale pore systems by porosimetry, pycnometry, surface area, and field emission scanning electron microscopy/transmission electron microscopy image analyses: examples from the Barnett, Woodford, Haynesville, Marcellus, and Doig units," *AAPG Bulletin*, vol. 96, no. 6, pp. 1099–1119, 2012.

[36] L. F. Ruppert, R. Sakurovs, T. P. Blach et al., "A USANS/SANS study of the accessibility of pores in the Barnett shale to methane and water," *Energy & Fuels*, vol. 27, no. 2, pp. 772–779, 2013.

[37] J. L. Zhao, M. D. Sun, Z. J. Pan, B. Liu, M. Ostadhassan, and Q. H. Hu, "Effects of pore connectivity and water saturation on matrix permeability of deep gas shale," *Advances in Geo-Energy Research*, vol. 6, no. 1, pp. 54–68, 2022.

[38] H. Dehghanpour, Q. Lan, Y. Saeed, H. Fei, and Z. Qi, "Spontaneous imbibition of brine and oil in gas shales: effect of water adsorption and resulting microfractures," *Energy & Fuels*, vol. 27, no. 6, pp. 3039–3049, 2013.

[39] A. Merkel, R. Fink, and R. Littke, "The role of pre-adsorbed water on methane sorption capacity of bossier and Haynesville shales," *International Journal of Coal Geology*, vol. 147-148, pp. 1–8, 2015.

[40] J. Li, X. F. Li, Y. Y. Li et al., "Model for gas transport in nanopores of shale and tight formation under reservoir condition," *Chinese Journal of Theoretical and Applied Mechanics*, vol. 47, pp. 932–944, 2015.

[41] S. B. Chen, Z. Gong, X. Y. Li, H. J. Wang, Y. Wang, and Y. K. Zhang, "Pore structure and heterogeneity of shale gas reservoirs and its effect on gas storage capacity in the Qiongzhusi Formation," *Geoscience Frontiers*, vol. 12, no. 6, article 101244, 2021.

[42] Y. Wang, H. F. Cheng, Q. H. Hu et al., "Pore structure heterogeneity of Wufeng-Longmaxi shale, Sichuan Basin, China: evidence from gas physisorption and multifractal geometries," *Journal of Petroleum Science and Engineering*, vol. 208, article 109313, 2022.

[43] J. G. Wu, Y. Yuan, S. Y. Niu, X. F. Wei, and J. J. Yang, "Multi-scale characterization of pore structure and connectivity of Wufeng-Longmaxi shale in Sichuan Basin, China," *Marine and Petroleum Geology*, vol. 120, article 104514, 2020.

[44] W. Guo, Y. B. Yao, D. M. Liu, X. X. Sun, and Y. W. Gao, "Research on measurement of pores in coals with NMRC technique," *Oil & Gas Geology*, vol. 37, pp. 141–148, 2016.

[45] Z. Q. Li, Z. Y. Qi, X. Shen, R. L. Hu, R. Q. Huang, and Q. Han, "Research on quantitative analysis for nanopore structure characteristics of shale based on NMR and NMR cryoporometry," *Energy & Fuels*, vol. 31, no. 6, pp. 5844–5853, 2017.

[46] J. Mitchell, J. B. W. Webber, and J. H. Strange, "Nuclear magnetic resonance cryoporometry," *Physics Reports*, vol. 461, no. 1, pp. 1–36, 2008.

[47] O. V. Petrov and I. Furo, "NMR cryoporometry: principles, applications and potential," *Progress in Nuclear Magnetic Resonance Spectroscopy*, vol. 54, no. 2, pp. 97–122, 2009.

[48] C. L. Jackson and G. B. McKenna, "The melting behavior of organic materials confined in porous solids," *Journal of Chemical Physics*, vol. 93, no. 12, pp. 9002–9011, 1990.

[49] T. J. Rottreau, C. M. A. Parlett, A. F. Lee, and R. Evans, "NMR cryoporometric measurements of porous silica: a method for the determination of melting point depression parameters of probe liquids," *Microporous and Mesoporous Materials*, vol. 264, pp. 265–271, 2018.

[50] B. Liu, S. P. Yao, W. X. Hu, and J. Cao, "Applying octamethylcyclotetrasiloxane as a probe liquid for characterizing the pore size distribution of oil-bearing tight sandstones by nuclear magnetic resonance cryoporometry," *Marine and Petroleum Geology*, vol. 88, pp. 814–825, 2017.

[51] Y. Qin, S. P. Yao, H. M. Xiao et al., "Pore structure and connectivity of tight sandstone reservoirs in petroleum basins: a review and application of new methodologies to the late Triassic Ordos Basin, China," *Marine and Petroleum Geology*, vol. 129, article 105084, 2021.

[52] Y. X. Zhao, Y. F. Sun, S. M. Liu, K. Wang, and Y. D. Jiang, "Pore structure characterization of coal by NMR cryoporometry," *Fuel*, vol. 190, pp. 359–369, 2017.

[53] Y. X. Zhao, L. Peng, S. M. Liu, B. Cao, Y. F. Sun, and B. F. Hou, "Pore structure characterization of shales using synchrotron SAXS and NMR cryoporometry," *Marine and Petroleum Geology*, vol. 102, pp. 116–125, 2019.

[54] B. Zhou, Q. Han, and P. Q. Yang, "Characterization of nanoporous systems in gas shales by low field NMR cryoporometry," *Energy & Fuels*, vol. 30, no. 11, pp. 9122–9131, 2016.

[55] F. Zhu, W. X. Hu, J. Cao, F. N. Sun, Y. F. Liu, and Z. M. Sun, "Micro/nanoscale pore structure and fractal characteristics of tight gas sandstone: a case study from the Yuanba area, northeast Sichuan Basin, China," *Marine and Petroleum Geology*, vol. 98, pp. 116–132, 2018.

[56] L. B. Lin, Y. Yu, C. B. Zhai et al., "Paleogeography and shale development characteristics of the Late Permian Longtan Formation in southeastern Sichuan Basin, China," *Marine and Petroleum Geology*, vol. 95, pp. 67–81, 2018.

[57] Y. H. Fu, Y. Q. Jiang, Z. L. Wang et al., "Non-connected pores of the Longmaxi shale in southern Sichuan Basin of China," *Marine and Petroleum Geology*, vol. 110, pp. 420–433, 2019.

[58] W. Li, L. A. Stevens, C. N. Uguna et al., "Comparison of the impact of moisture on methane adsorption and nanoporosity for over mature shales and their kerogens," *International Journal of Coal Geology*, vol. 237, article 103705, 2021.

[59] A. Zolfaghari, H. Dehghanpour, and J. Holyk, "Water sorption behaviour of gas shales: I. Role of clays," *International Journal of Coal Geology*, vol. 179, pp. 130–138, 2017.

[60] Q. Zhang, Y. H. Dong, S. M. Liu, D. Elsworth, and Y. X. Zhao, "Shale pore characterization using NMR cryoporometry with octamethylcyclotetrasiloxane as the probe liquid," *Energy & Fuels*, vol. 31, no. 7, pp. 6951–6959, 2017.

[61] C. Cadar, C. Cotet, L. Baia, L. B. Tudoran, and I. Ardelean, "Probing into the mesoporous structure of carbon xerogels via the low-field NMR relaxometry of water and cyclohexane molecules," *Microporous and Mesoporous Materials*, vol. 251, pp. 19–25, 2017.

[62] Q. Zhang, Y. H. Dong, S. Q. Tong, X. Li, and L. H. Wang, "Nuclear magnetic resonance cryoporometry as a tool to measure pore size distribution of shale rock," *Chinese Science Bulletin*, vol. 61, no. 21, pp. 2387–2394, 2016.